

Synthesis and thermoelectric properties of Bi-doped SnSe thin films

Jun Pang(庞军), Xi Zhang(张析)†, Limeng Shen(申笠蒙), Jiayin Xu(徐家胤), Ya Nie(聂娅), and Gang Xiang(向钢)
Citation: Chin. Phys. B, 2021, 30 (**11**): 116302. DOI: 10.1088/1674-1056/ac11da
Journal homepage: http://cpb.iphy.ac.cn; http://iopscience.iop.org/cpb

What follows is a list of articles you may be interested in

Two-dimensional MnN utilized as high-capacity anode for Li-ion batteries

Junping Hu(胡军平), Zhangyin Wang(王章寅), Genrui Zhang(张根瑞), Yu Liu(刘宇), Ning Liu(刘宁), Wei Li(李未), Jianwen Li(李健文), Chuying Ouyang(欧阳楚英), and Shengyuan A. Yang(杨声远)
Chin. Phys. B, 2021, 30 (**4**): 046302. DOI: 10.1088/1674-1056/abdda8

Effect of strain on electrochemical performance of Janus MoSSe monolayer anode material for Li-ion batteries: First-principles study

Guoqing Wang(王国庆), Wenjing Qin(秦文静), and Jing Shi(石晶)
Chin. Phys. B, 2021, 30 (**4**): 046301. DOI: 10.1088/1674-1056/abca24

First-principles study of the co-effect of carbon doping and oxygen vacancies in ZnO photocatalyst

Jia Shi(史佳), Lei Wang(王蕾), and Qiang Gu(顾强)
Chin. Phys. B, 2021, 30 (**2**): 026301. DOI: 10.1088/1674-1056/abc0db

Surface-regulated triangular borophene as Dirac-like materials from density functional calculation investigation

Wenyu Fang(方文玉), Wenbin Kang(康文斌), Jun Zhao(赵军), Pengcheng Zhang(张鹏程)
Chin. Phys. B, 2020, 29 (**9**): 096301. DOI: 10.1088/1674-1056/ab9bff

Physical properties of ternary thallium chalcogenes Tl_2MQ_3 (M=Zr, Hf; Q=S, Se, Te) via *ab-initio* calculations

Engin Ateser, Oguzhan Okvuran, Yasemin Oztekin Ciftci, Haci Ozisik, Engin Deligoz
Chin. Phys. B, 2019, 28 (**10**): 106301. DOI: 10.1088/1674-1056/ab427d

---

Synthesis and thermoelectric properties of Bi-doped SnSe thin films*

Jun Pang(庞军), Xi Zhang(张析)†, Limeng Shen(申笠蒙),
Jiayin Xu(徐家胤), Ya Nie(聂娅), and Gang Xiang(向钢)‡

College of Physics, Sichuan University, Chengdu 610064, *China*

(Received 16 February 2021; revised manuscript received 19 June 2021; accepted manuscript online 7 July 2021)

Bi doped n-type SnSe thin films were prepared by chemical vapor deposition (CVD) and their structure and thermoelectric properties were studied. The x-ray diffraction patterns, x-ray photoelectron spectroscopy, and microscopic images show that the prepared SnSe thin films were composed of pure SnSe crystals. The Seebeck coefficients of the Bi-doped SnSe were greatly improved compared to that of undoped SnSe thin films. Specifically, $Sn_{0.99}Bi_{0.01}Se$ thin film exhibited a Seebeck coefficient of -905.8 $\mu V \cdot K^{-1}$ at 600 K, much higher than 285.5 $\mu V \cdot K^{-1}$ of undoped SnSe thin film. Further first-principles calculations reveal that the enhancement of the thermoelectric properties can be explained mainly by the Fermi level lifting and the carrier pockets increasing near the Fermi level due to Bi doping in the SnSe samples. Our results suggest the potentials of the Bi-doped SnSe thin films in thermoelectric applications.

Keywords: SnSe thin films, Bi doping, thermoelectric properties, Seebeck coefficient

PACS: 63.20.dk, 73.50.Lw, 68.35.bg **DOI:** 10.1088/1674-1056/ac11da

1. Introduction

Thermoelectric (TE) materials, enabling energy conversion between heat and electricity,[1,2] offer a possibility for electricity generation and refrigeration.[3–7] The efficiency of TE materials is usually measured by power factor (σS^2) and a dimensionless figure of merit, which is defined as $ZT = \sigma S^2 T/\kappa$, where σ is the electrical conductivity, S is the Seebeck coefficient, T is the absolute temperature, and κ is the thermal conductivity, respectively. A high σS^2 or a low κ is required for excellent thermoelectric materials. There are three strategies to optimize ZT values. First, the Seebeck coefficient can be increased through carrier doping or energy filtering of charge carriers.[8,9] Second, the electrical conductivity can be increased by lowering the effective mass of the carriers or modulation doping in a quantum well.[10,11] Third, the thermal conductivity can be reduced by adding interfaces and phonon scattering centers in a nanowire, nanotube, superlattice, alloy or composite.[12,13] Such methods are typically used in the synthesis of excellent polycrystalline thermoelectric materials.

As a new generation of thermoelectric materials with great potential, SnSe and its related thermoelectric materials have drawn extensive attention for its excellent thermoelectric properties.[14–20] For example, Zhao *et al*. reported that p-type SnSe single crystals exhibited ultralow thermal conductivity and an outstanding ZT value of 2.6 at 923 K.[15] Bi doped n-type SnSe single crystals also showed a high ZT value of 2.2 at 733 K.[16] Ge *et al*. found that Re and Cl co-doping could significantly enhance the electrical transport performance and reduce the thermal conductivity of n-type SnSe bulk samples, which results in a ZT value of 1.5 at 793 K.[18] As we know, thin film fabrication is important for modern micro- and nano-devices since thin film materials can be easily incorporated into complex structures for various applications.[21] Because of this, SnSe thin films have been extensively investigated and shown great potentials in the fields of miniaturized optoelectronic, photovoltaic, and thermoelectric devices.[22–24] At the same time, researches have shown that the thermoelectric and optoelectronic properties of p-type SnSe thin films can be improved by doping suitable elements such as Ag, Co, Pb, and Zn.[25–27] At the same time, n-type Bi-doped SnSe bulk samples have been studied and exhibited good thermoelectric properties.[16,28] However, the report on the synthesis of n-type SnSe thin films, especially Bi-doped SnSe thin films, is rare.

In this work, we synthesized Bi-doped n-type SnSe thin films by chemical vapor deposition and investigated the thermoelectric properties of Bi-doped SnSe thin films. Our data show that the Seebeck coefficient of the Bi-doped SnSe thin films reaches a maximum absolute value of -905.8 $\mu V \cdot K^{-1}$ at 600 K. Further first-principles calculations indicate that appropriate Bi-doping can shift the Fermi level up in the energy band and improve the overall thermoelectric performance of the SnSe thin films. Our results suggest the potentials of n-type SnSe thin films in the thermoelectric application.

2. Experimental and theoretical methods

SnSe powder (purity 99.999%, 100 mg) was first evenly mixed with different amount of Bi powder (purity 99.999%, 0, 2.5, 3, 4 mg), then the mixed powder was placed in the

*Project supported by the National Key Research and Development Program of China (Grant No. 2017YFB0405702) and the National Natural Science Foundation of China (Grant No. 51672179).

†Corresponding author. E-mail: xizhang@scu.edu.cn

‡Corresponding author. E-mail: gxiang@scu.edu.cn

© 2021 Chinese Physical Society and IOP Publishing Ltd

center of the high-temperature zone in the CVD system as the source. A piece of intrinsic Si (100) was placed in the low-temperature zone as the substrate to grow continuous SnSe thin films. The mixed powder was heated to 1100 K at a rate of 20 K·min^{-1}, and the low-temperature zone was heated to 900 K at a rate of 15 K·min^{-1}. Ar (5% H_2) gas with a flow ratio of 40-standard cubic centimeter per minute (SCCM) was introduced as the carrier gas. The pressure was adjusted to 10 Torr (1 Torr = 1.33322×10^2 Pa) during the film growth. After a growth duration of 40 min, the system was cooled to room temperature naturally.

Density functional theory (DFT) was used to calculate electronic properties of the SnSe samples, which is implemented in Vienna *ab initio* simulation package (VASP)[29–31] with the projector augmented wave (PAW) method. The exchange–correlation functional was defined using a generalized gradient approximation (GGA) of Perdew–Burke–Ernzerhof (PBE).[32] A supercell with 48 Sn atoms and 48 Se atoms ($3 \times 2 \times 2$, *Pnma*) was built, and a Sn atom was randomly replaced with a Bi atom corresponding to a doping concentration of 2%. The plane wave cutoff was set to 520 eV, and a Monkhorst–Pack *k*-mesh of $3 \times 3 \times 3$ was used to sample the Brillouin zone (BZ) for integrations in reciprocal space. Both atomic positions and lattice constants were fully relaxed until the magnitude of the force acting on all atoms became less than 0.01 eV·Å^{-1} and electronic convergence threshold for energy was set to be 10^{-5} eV.

The crystal structures were analyzed by x-ray diffraction (XRD, Fangyuan, DX-2500) with a Cu $K\alpha$ ($\lambda = 0.15418$ nm) radiation source. X-ray photoelectron spectroscopy (XPS, Thermo Scientific Escalab 250Xi) measurement was carried out to study the chemical state of the sample. The morphologies of the Bi-doped SnSe thin films were characterized by scanning electron microscopy (SEM, Thermo Scientific, Apreo-S). The elementary compositions of the SnSe film were investigated by energy dispersive x-ray spectrometry (EDS, Oxford, X-MaxN 80). The microstructures were characterized by high resolution transmission electron microscope (HRTEM, FEI Tecnai, G2 F20). The electrical properties of the samples were measured using a van der Pauw method in an east changing magneto-transport equipment (ET9007). The Seebeck coefficient was measured by an SB1000 Seebeck measurement system with K2000 digital temperature controller. Owing to its high resistivity, the intrinsic silicon substrate can be viewed as an insulator that has little effect on the electrical conductivities of our samples.

3. Results and discussion

The structures of the synthsized SnSe thin films were first studied. The XRD patterns of undoped and Bi-doped SnSe thin films with different Bi concentration x ($x = 0$, 0.005, 0.01, 0.02) were shown in Fig. 1(a). The actual elemental compositions of the samples were obtained from energy dispersive x-ray spectrometry. The major diffraction peaks can be well indexed to the orthorhombic SnSe (JCPDS: 48-1224). The obvious difference in relative diffraction intensity in (400) and (111) planes indicates the existence of anisotropy of the samples. Owing to the substitution of a smaller atom Sn by a bigger atom Bi, the peak positions of the $Sn_{0.99}Bi_{0.01}Se$ sample shift a little bit to smaller angles with respect to that of the undoped sample. However, the peak positions of $Sn_{0.98}Bi_{0.02}Se$ sample shift toward bigger angles, which indicates that some of Bi ions may be incorporated into the lattice interstitial of SnSe, which were also observed in other studies.[28,33]

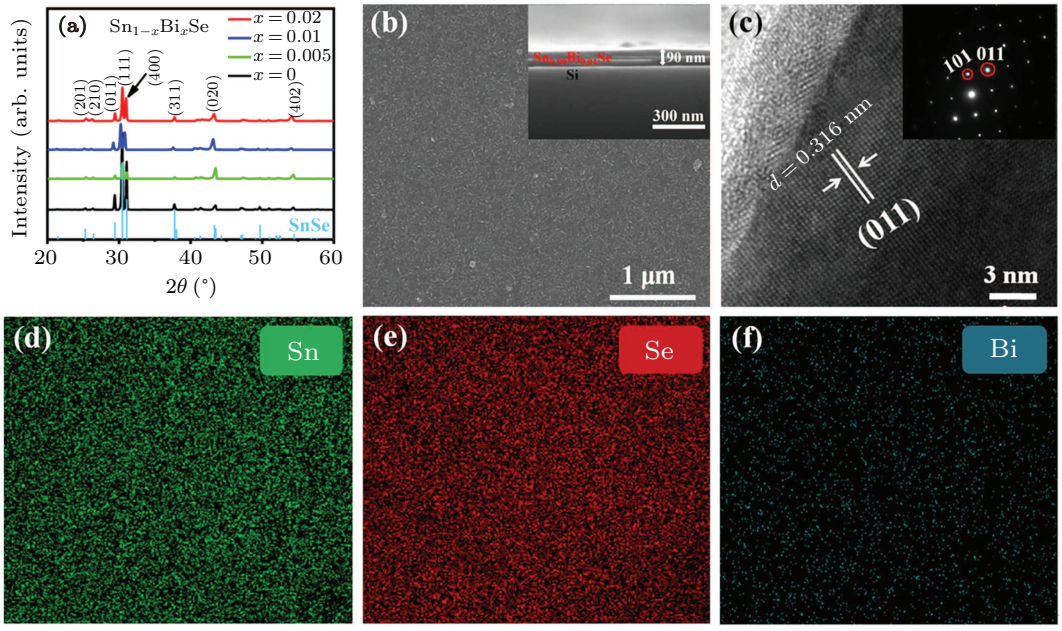


Fig. 1. (a) XRD of undoped and Bi-doped SnSe thin films. (b) SEM image and the inset shows the cross-section SEM image of $Sn_{0.99}Bi_{0.01}Se$ thin film. (c) HRTEM image and the inset shows the corresponding SAED of $Sn_{0.99}Bi_{0.01}Se$ thin film. (d)–(f) EDS mapping images of Sn, Se, and Bi from $Sn_{0.99}Bi_{0.01}Se$ thin film.

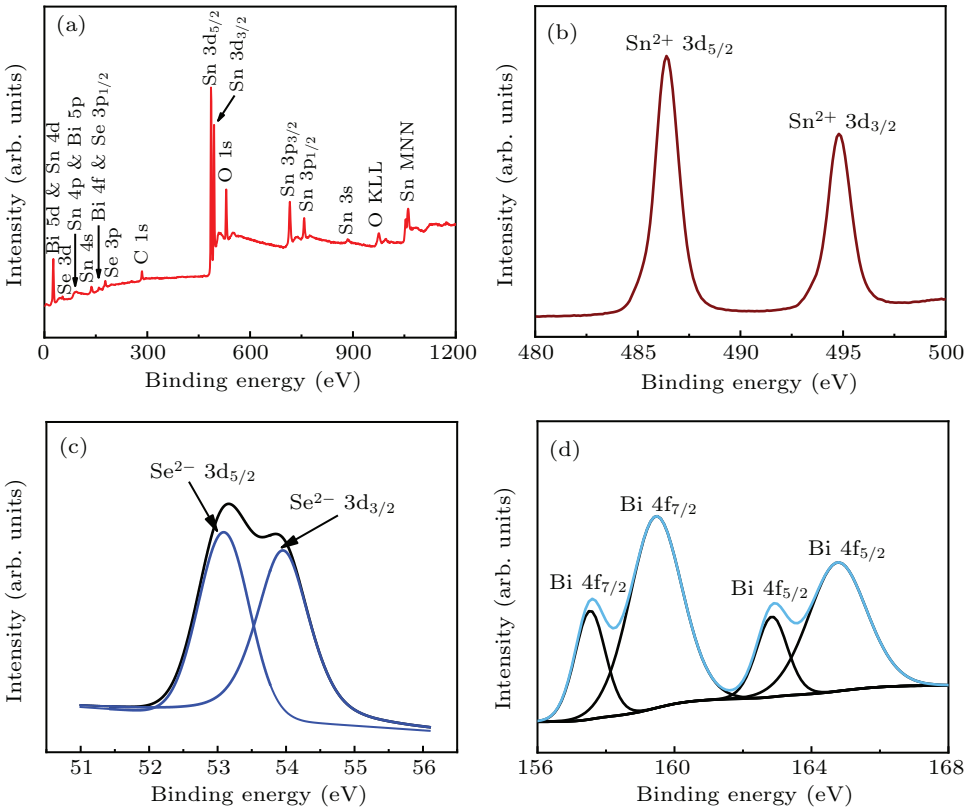


Fig. 2. XPS of $Sn_{0.99}Bi_{0.01}Se$ thin film. (a) Survey scans and high-resolution scans of (b) Sn 3d, (c) Se 3d, and (d) Bi 4f in $Sn_{0.99}Bi_{0.01}Se$ thin film.

In Fig. 1(b), the SEM image shows that our film is uniform except some dots formed on it. EDS mapping shows that the Bi concentration of white dots is same as that of the thin film (not shown). The total thickness of our thin film was also measured and estimated as 90 nm as shown in the cross-section SEM image. Further structural characterizations were performed by using high-resolution transmission electron microscope. Figure 1(c) reveals that the layer distance is 0.316 nm, corresponding to that of the (011) face of SnSe. The corresponding selected area electron diffraction (SAED) data exhibit a clear orthogonally symmetric spot pattern, as shown in the inset of Fig. 1(c), indicating the high phase purity and high crystallinity of the SnSe thin film. Figures 1(d)–1(f) show the EDS mapping images of Sn, Se, and Bi from $Sn_{0.99}Bi_{0.01}Se$ film, we can see that the elementary distribution of the Bi-doped SnSe film is uniform.

The composition and the chemical states of Bi-doped SnSe thin films were then studied by x-ray photoelectron spectroscopy (XPS). In Fig. 2(a), the XPS survey scan of the sample shows the presence of Sn, Se, Bi, C, and O in a typical Bi-doped thin film ($Sn_{0.99}Bi_{0.01}Se$). In Fig. 2(b), the Sn 3d spin–orbit doublet peaks appear at 486.42 eV and 494.81 eV with splitting of 8.4 eV, which can be assigned to Sn $3d_{5/2}$ and Sn $3d_{3/2}$,[34] respectively. Figure 2(c) shows the broad peak of Se can be deconvoluted as Se $3d_{5/2}$ and Se $3d_{3/2}$ peaks at binding energies of 53.10 eV and 53.96 eV, respectively.[35] In Fig. 2(d), the presence of Bi $4f_{7/2}$ and Bi $4f_{5/2}$ peaks at 157.6 eV and 162.9 eV can be attributed to Bi^{3+} states in Bi-doped SnSe sample,[28,34] while the peaks at 159.48 eV and 164.76 eV belong to the Bi^{5+} ions.[36] Considering the facts the XRD patterns show peak shifting owing to the Bi-doping and EDS mappings indicate that Bi elements were evenly distributed in the sample, the XPS results agree with the previous analysis.

Then the thermoelectric properties of the Bi-doped SnSe thin films were characterized in Fig. 3. Figure 3(a) shows the temperature-dependent Seebeck coefficients (S) for $Sn_{1-x}Bi_xSe$ ($x = 0$, 0.005, 0.01, 0.02) thin films. The undoped SnSe shows positive S values but three Bi-doped SnSe show negative S values. The reason for positive S value in undoped SnSe is that undoped SnSe samples often have Sn vacancy defects unavoidably generated during growth, and exhibit p-type characteristics.[16,37,38] The reason for negative S value in Bi-doped SnSe is that the Bi-dopants are donors and will generate electrons in SnSe, which makes SnSe change from p-type to n-type. If one look at the absolute S values, the temperature dependencies of the absolute S values of Bi doped SnSe are similar to that of the undoped SnSe, in which the absolute S values decrease as the temperature increases above 600 K due to the so called bipolar transport.[15,39] The maximal S value is achieved as $-905.8\ \mu V{\cdot}K^{-1}$ at 600 K in $Sn_{0.99}Bi_{0.01}Se$ thin film, which is better than previously reported values of $-400\ \mu V{\cdot}K^{-1}$ to $-900\ \mu V{\cdot}K^{-1}$ in high-quality Bi-doped SnSe crystalline bulks at 300 K–700 K.[16,28] Since the lattice mismatch $\varepsilon = (a_{si} - a_{SnSe})/a_{si}$ between the SnSe thin film and Si substrate is negative and n-type See-

beck coefficient can be increased by compressive strain,[40] the higher S value of our n-type SnSe thin films is probably owing to the compressive strain between the SnSe thin films and the Si substrate. As shown in Fig. 3(b), the electrical conductivity (σ) of undoped SnSe and Bi-doped SnSe shows different trends. The explanations are as follows. As to the undoped SnSe, the σ value first increases with increasing temperature up to 450 K owing to the thermal excitation of minority carriers, and then starts to decrease from 450 K owing to the formation of deep level defects,[41] which is like those observed in undoped SnSe bulks.[28,42] The σ values of all the Bi-doped SnSe samples show increasing trends as the temperature increases up to 700 K, since Bi dopants decrease the deep level defect concentration by suppressing the formation of traps.[43,44] Doping n-type dopant Bi into p-type SnSe will decrease the electrical conductivity first, which is accompanied by the decreased Hall carrier concentration, as shown in Fig. 3(d). The carrier type changes from hole to electron and carrier concentration decreases from 6.14×10^{17} cm^{-3} to 1.36×10^{17} cm^{-3} when the undoped SnSe (more accurately, p-type unintentionally doped) is doped and become n-type $Sn_{0.995}Bi_{0.005}Se$ with 0.5% Bi dopants, owing to the electrons generated by Bi dopants. After that, the carrier type remain electron and carrier concentration keep increasing as Bi doping concentration increases. Meanwhile, the Hall mobility of carrier first increases owing to less carrier scattering resulted from the neutralization effect between n-type Bi dopants and unintentionally doped p-type defects, and then decreases owing to more and more carrier scattering when the Bi doping concentration increases. It is noted that the mobility of the SnSe thin film is lower than that of bulk materials,[28,45] which is probably caused by the phonon scattering at the surface and grain boundary in the thin films.

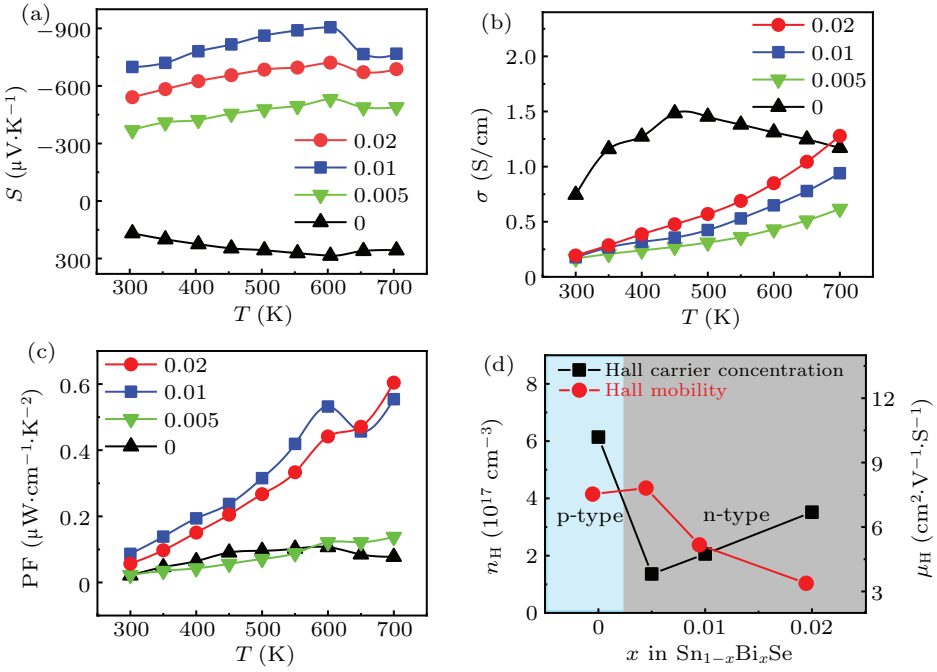


Fig. 3. Temperature-dependent (a) Seebeck coefficient, (b) electrical conductivity, (c) power factor (σS^2), and (d) room-temperature Hall carrier concentration and Hall mobility of $Sn_{1-x}Bi_xSe$ ($x = 0$, 0.005, 0.01, 0.02) thin films.

Figure 3(c) shows the temperature-dependent PF of different SnSe thin films. Low PF values with small variations are obtained in undoped SnSe and $Sn_{0.995}Bi_{0.005}Se$ thin films due to their low Seebeck coefficients. Owing to the significant increase of Seebeck coefficient, the higher PF values are obtained in $Sn_{0.99}Bi_{0.01}Se$ and $Sn_{0.98}Bi_{0.02}Se$ thin films. Specifically, the PF value reaches a maximum of 0.6 μW·cm^{-1}·K^{-2} at 700 K when Bi doping concentration is 2%.

In fact, the measurement of thermal conductivity of thin films is notoriously difficult.[46–48] As other groups have pointed out, thin films are usually expected to have lower thermal conductivity than their bulk counterparts due to the phonon scattering at the surface and grain boundary, and hence many of them have used the thermal conductivity of the corresponding bulk materials to estimate the lower bound of ZTs of the thin films.[46–48] At the same time, previous studies have shown that the thermal conductivity of Bi-doped SnSe bulk samples is comparable to or even lower than that of bulk SnSe.[16,49,50] Therefore, we use the thermal conductivity of the bulk polycrystalline SnSe reported in the literature[51] to estimate the lower bound of ZTs of our Bi-doped SnSe films. Temperature dependence of the thermal conductivity of the bulk polycrystalline SnSe is shown in Fig. 4, owing to the fact that phonon scattering increases gradually with increasing temperature, κ decreases with increasing temperature. The conservatively estimate ZT values as a function

of temperature for all samples are shown in Fig. 4. The ZT values of $Sn_{0.99}Bi_{0.01}Se$ and $Sn_{0.98}Bi_{0.02}Se$ are significantly improved compared to that of pristine SnSe, which can be attributed to enhanced PF values. The obtained maximum ZT of $Sn_{0.98}Bi_{0.02}Se$ is 0.074 at 700 K. As discussed earlier, the actual ZT of our SnSe thin film may be higher than the estimated value here.

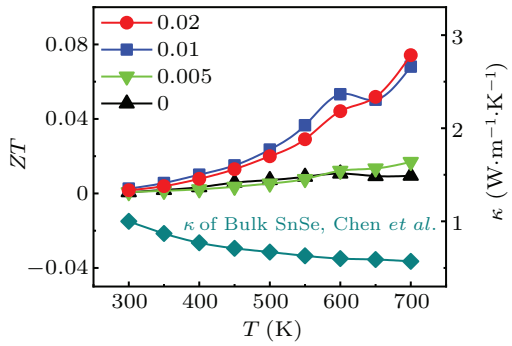


Fig. 4. Temperature-dependent figure of merit (ZT) for the $Sn_{1-x}Bi_xSe$ ($x = 0$, 0.005, 0.01, 0.02) thin films. The bottom curve is the total thermal conductivity of the reported bulk SnSe,[51] which is used to conservatively estimate the ZT of our SnSe thin films.

Since the Seebeck coefficients of $Sn_{0.99}Bi_{0.01}Se$ and $Sn_{0.98}Bi_{0.02}Se$ are improved dramatically compared to that of undoped SnSe, we calculated their electronic structures to understand the effect of Bi-doping on the thermoelectric properties of the SnSe samples. Figure 5 shows the comparison between the pristine SnSe sample and a typical Bi-doped SnSe sample ($Sn_{0.98}Bi_{0.02}Se$). The density of states (DOSs) near the Fermi level are mainly composed of the s-orbitals and p-orbitals of Sn, and the p-orbitals of Se. After doping Bi into SnSe, the Fermi level is shifted up into the conduction band, and hence the DOSs near the Fermi level is increased and Bi-doped SnSe become n-type, as shown Fig. 5. According to Mott expression,[52] the increase in the local DOSs near the Fermi level can enhance the Seebeck coefficient. The band structure of $Sn_{0.98}Bi_{0.02}Se$ is shown in Fig. 5(d) where four conduction bands named CB1, CB2, CB3, and CB4 are near the Γ point in the Brillouin zone. The differences between the four band energies are on the order of k_BT, suggesting that doping Bi into SnSe will introduce some carrier pockets near the Fermi level. Previous studies have shown that the increase of carrier pockets near the Fermi level will also improve the Seebeck coefficient.[53–55] Therefore, doping Bi into SnSe is indeed an effective way to improve the thermoelectric properties of SnSe. The results of theoretical calculations agree well with the experimental results.

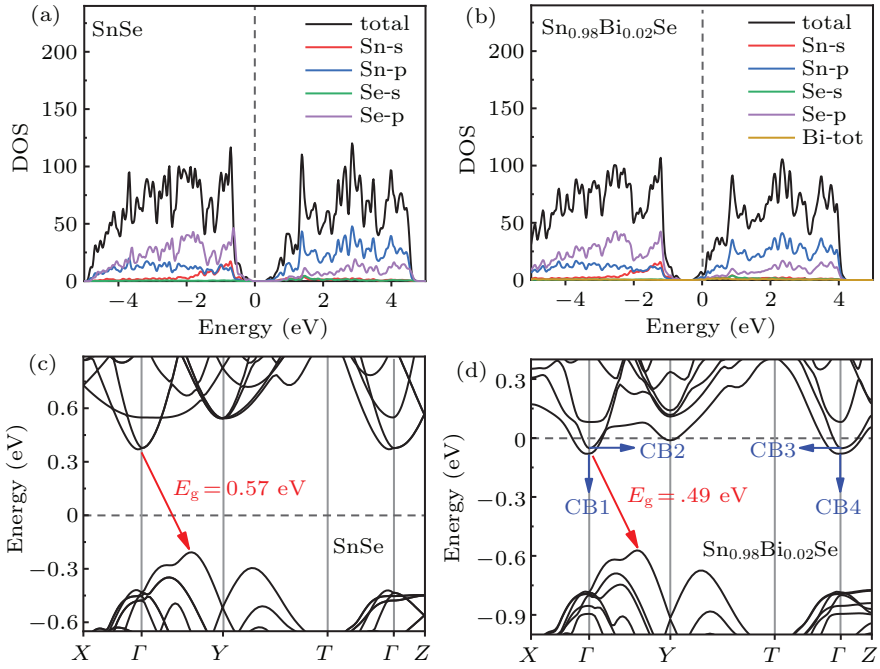


Fig. 5. [(a) and (b)] DOSs and [(c) and (d)] electronic band structures of the undoped SnSe and $Sn_{0.98}Bi_{0.02}Se$ samples.

4. Conclusion

In this work, Bi-doped SnSe thin films were prepared on Si substrate by CVD and their structures and thermoelectric properties were studied. The ZT values of $Sn_{0.99}Bi_{0.01}Se$ and $Sn_{0.98}Bi_{0.02}Se$ thin films are significantly improved compared to that of pristine SnSe, which can be attributed to the enhanced PF values. The obtained maximum ZT of $Sn_{0.98}Bi_{0.02}Se$ thin film is 0.074 at 700 K. The enhancement of the thermoelectric properties is related to the Fermi level lifting and the carrier pockets increasing near the Fermi level due to Bi doping in the SnSe samples. Our results thus provide an effective way to improve the thermoelectric properties of SnSe thin films.

Acknowledgements

We are very grateful to the help from the Analytical and Testing Center of Sichuan University.

References

[1] Bell L E 2008 *Science* **321** 1457
[2] Sootsman J R, Chung D Y and Kanatzidis M G 2009 *Angew. Chemie - Int. Ed.* **48** 8616
[3] Snyder G J and Toberer ES 2008 *Nat. Mater.* **7** 105
[4] Poudel B, Hao Q, Ma Y, Lan Y, Minnich A, Yu B, Yan X, Wang D, Muto A, Vashaee D, Chen X, Liu J, Dresselhaus M S, Chen G and Ren Z 2008 *Science* **320** 634
[5] Dresselhaus M S, Chen G, Tang M Y, Yang R, Lee H, Wang D, Ren Z, Fleurial J P and Gogna P 2007 *Adv. Mater.* **19** 1043
[6] Biswas K, He J, Blum I D, Wu C I, Hogan T P, Seidman D N, Dravid V P and Kanatzidis M G 2012 *Nature* **489** 414
[7] Liu Y, Lu J, Wang R, Wang C and Jiang J H 2020 *Chin. Phys. B* **29** 040504
[8] Paul B and Banerji P 2009 *Nanosci. Nanotechnol. Lett.* **1** 208
[9] Heremans J P, Jovovic V, Toberer E S, Saramat A, Kurosaki K, Charoenphakdee A, Yamanaka S and Snyder G J 2008 *Science.* **321** 1457
[10] Goldsmid H J 2012 *J. Electron. Mater.* **41** 2126
[11] Yu B, Zebarjadi M, Wang H, Lukas K, Wang H, Wang D, Opeil C, Dresselhaus M, Chen G and Ren Z 2012 *Nano Lett.* **12** 2077
[12] Liu W, Hu J, Zhang S, Deng M, Han C G and Liu Y 2017 *Mater. Today Phys.* **1** 50
[13] Li W, Chen Z, Lin S, Chang Y, Ge B, Chen Y and Pei Y 2015 *J. Mater.* **1** 307
[14] Zhao L D, Tan G, Hao S, He J, Pei Y, Chi H, Wang H, Gong S, Xu H, Dravid V P, Uher C, Snyder G J, Wolverton C and Kanatzidis M G 2016 *Science* **351** 141
[15] Zhao L D, Lo S H, Zhang Y, Sun H, Tan G, Uher C, Wolverton C, Dravid V P and Kanatzidis M G 2014 *Nature* **508** 373
[16] Duong A T, Nguyen V Q, Duvjir G, Duong V T, Kwon S, Song J Y, Lee J K, Lee J E, Park S, Min T, Lee J, Kim J and Cho S 2016 *Nat. Commun.* **7** 1
[17] Feng Y Y, Zhang X, Lei L, Nie Y and Xiang G 2020 *RSC Adv.* **10** 11990
[18] Ge Z H, Qiu Y, Chen Y X, Chong X, Feng J, Liu Z K and He J 2019 *Adv. Funct. Mater.* **29** 1
[19] Yan S S, Wang Y, Gao Z B, Long Y and Ren J 2021 *Chin. Phys. Lett.* **38** 027301
[20] Zhou L Y, Zheng Q, Bao L H and Liang W J 2020 *Chin. Phys. Lett.* **37** 017301
[21] Wang Q H, Kalantar-Zadeh K, Kis A, Coleman J N and Strano M S 2012 *Nat. Nanotechnol.* **7** 699
[22] Vaughn D D, In S Il and Schaak R E 2011 *ACS Nano* **5** 8852
[23] Hao L, Wang Z, Xu H, Yan K, Dong S, Liu H, Du Y, Wu Y, Liu Y and Dong M 2019 *2D Mater.* **6** 034004
[24] Xu H, Hao L, Liu H, Dong S, Wu Y, Liu Y, Cao B, Wang Z, Ling C, Li S, Xu Z, Xue Q and Yan K 2020 *ACS Appl. Mater. Interfaces* **12** 35250
[25] Liu S, Sun N, Liu M, Sucharitakul S and Gao X P A 2018 *J. Appl. Phys.* **123** 115109
[26] Liu S, Lan M, Li G, Yuan Y, Jia B and Wang Q 2020 *Ceram. Int.* **46** 16578
[27] Jamali-Sheini F, Cheraghizade M and Yousefi R 2018 *Appl. Surf. Sci.* **443** 345
[28] Li X F, Chen C, Xue W H, Li S, Cao F, Chen Y X, He J Q, Sui J H, Liu X J, Wang Y M and Zhang Q 2018 *Inorg. Chem.* **57** 13800
[29] Kohn W and Sham L J 1965 *Phys. Rev.* **140** A1133
[30] Kresse G and Hafner J J 1993 *Phys. Rev. B* **48** 13115
[31] Blöchl P E 1994 *Phys. Rev. B* **50** 17953
[32] Perdew J P, Burke K and Ernzerhof M 1996 *Phys. Rev. Lett.* **77** 3865
[33] Montazeri A and Jamali-Sheini F 2017 *Sensors Actuators, B Chem.* **242** 778
[34] Banik A and Biswas K 2017 *Angew. Chemie* **129** 14753
[35] Saha S, Banik A and Biswas K 2016 *Chem.: A Eur. J.* **22** 15634
[36] Fan H, Wang G and Hu L 2010 *Solid State Sci.* **11** 2065
[37] Heo S H, Jo S, Kim H S, Choi G, Song J Y, Kang J Y, Park N J, Ban H W, Kim F, Jeong H, Jung J, Jang J, Lee W B, Shin H and Son J S 2019 *Nat. Commun.* **10** 1
[38] Duvjir G, Min T, Thi Ly T, Kim T, Duong A T, Cho S, Rhim S H, Lee J and Kim J 2017 *Appl. Phys. Lett.* **110** 262106
[39] Shi G and Kioupakis E 2015 *J. Appl. Phys.* **117** 065103
[40] Guo D, Hu C, Xi Y and Zhang K 2013 *J. Phys. Chem. C* **117** 21597
[41] Chen S, Cai K and Zhao W 2012 *Physica B* **407** 4154
[42] Liu J, Wang P, Wang M, Xu R, Zhang J, Liu J, Li D, Liang N, Du Y, Chen G and Tang G 2018 *Nano Energy* **53** 683
[43] Mooney P M, Watkins K P, Jiang Z, Basile A F, Lewis R B, Bahrami-Yekta V, Masnadi-Shirazi M, Beaton D A and Tiedje T 2013 *J. Appl. Phys.* **113** 133708
[44] Cheng Y, Chang Y, Feng Y, Jian H, Tang Z and Zhang H 2018 *Angew. Chemie Int. Ed.* **57** 246
[45] Zhao L D, Chang C, Tan G and Kanatzidis M G 2016 *Energy Environ. Sci.* **9** 3044
[46] Song L, Zhang J and Iversen B B 2019 *J. Mater. Chem. A* **7** 17981
[47] Song L, Zhang J and Iversen B B 2020 *ACS Appl. Energy Mater.* **3** 2055
[48] Zheng Z H, Fan P, Luo J T, Liang G X, Liu P J and Zhang D P 2016 *J. Alloys Compd.* **668** 8
[49] Chandra S, Banik A and Biswas K 2018 *ACS Energy Lett.* **3** 1153
[50] Nguyen V Q, Nguyen T H, Duong V T, Lee J E, Park S D, Song J Y, Park H M, Duong A T and Cho S 2018 *Nanoscale Res. Lett.* **13** 4
[51] Chen C L, Wang H, Chen Y Y, Day T and Snyder G J 2014 *J. Mater. Chem. A* **2** 11171
[52] Cutler M and Mott N F M 1969 *Phys. Rev.* **181** 1336
[53] Peng K, Lu X, Zhan H, Hui S, Tang X, Wang G, Dai J, Uher C, Wang G and Zhou X 2016 *Energy Environ. Sci.* **9** 454
[54] Zhao L D, Dravid V P and Kanatzidis M G 2014 *Energy Environ. Sci.* **7** 251
[55] Pei Y, Shi X, Lalonde A, Wang H, Chen L and Snyder G J 2011 *Nature* **473** 66